Key Points:
- Productivity in the equatorial Pacific generally decreased over the last 30 ka, particularly in the eastern and western equatorial Pacific subregions
- A deglacial productivity peak is only found in some records, particularly in the central and easternmost equatorial Pacific subregions

Productivity patterns in the equatorial Pacific over the last 30,000 years

Kassandra M. Costa[1,2] (iD), **Allison W. Jacobel[1,2]** (iD), **Jerry F. McManus[1,2]** (iD), **Robert F. Anderson[1,2]** (iD), **Gisela Winckler[1,2]** (iD)**, and Nivedita Thiagarajan[3]**

[1]Geochemistry Division, Lamont-Doherty Earth Observatory of Columbia University, Palisades, New York, USA, [2]Department of Earth and Environmental Sciences, Columbia University, New York, New York, USA, [3]Division of Geological and Planetary Sciences, California Institute of Technology, Pasadena, California, USA

Abstract The equatorial Pacific traverses a number of productivity regimes, from the highly productive coastal upwelling along Peru to the near gyre-like productivity lows along the international dateline, making it an ideal target for investigating how biogeochemical systems respond to changing oceanographic conditions over time. However, conflicting reconstructions of productivity during periods of rapid climate change, like the last deglaciation, render the spatiotemporal response of equatorial Pacific productivity ambiguous. In this study, surface productivity since the last glacial period (30,000 years ago) is reconstructed from seven cores near the Line Islands, central equatorial Pacific, and integrated with productivity records from across the equatorial Pacific. Three coherent deglacial patterns in productivity are identified: (1) a monotonic glacial-Holocene increase in productivity, primarily along the Equator, associated with increasing nutrient concentrations over time; (2) a deglacial peak in productivity ~15,000 years ago due to transient entrainment of nutrient rich southern-sourced deep waters; and (3) possible precessional cycles in productivity in the eastern equatorial Pacific that may be related to Intertropical Convergence Zone migration and potential interactions with El Niño–Southern Oscillation dynamics. These findings suggest that productivity was generally lower during the glacial period, a trend observed zonally across the equatorial Pacific, while deglacial peaks in productivity may be prominent only in the east.

1. Introduction

The equatorial Pacific comprises the largest tropical expanse of ocean on Earth today. Upwelling along the equator and in the eastern boundary current supplies surface waters with abundant nutrients that make this region an important biogeochemical province. In addition to upwelling, surface productivity may be influenced by a number of different processes related to El Niño–Southern Oscillation [*Lyle et al.*, 1988; *Turk et al.*, 2001; *Wang et al.*, 2006; *Park et al.*, 2011], Intertropical Convergence Zone (ITCZ) and seasonality [*Dandonneau et al.*, 2004; *Koutavas and Lynch-Stieglitz*, 2005], trace nutrient limitation (Fe and Si) [*Coale et al.*, 1996; *Moore et al.*, 2004; *Baines et al.*, 2011; *Brzezinski et al.*, 2011], and nutrient export from the Southern Ocean [*Sarmiento et al.*, 2004; *Liu and Alexander*, 2007; *Rafter et al.*, 2012; *Rafter and Sigman*, 2016]. The complex interplay of these processes may create zonal productivity gradients that, if identified and reconstructed, can provide insight into the relative sensitivities of the biological community to subtle changes in oceanographic conditions from east to west. Yet reconstructing the spatiotemporal patterns of productivity on orbital and suborbital time scales has been inconclusive.

Previous studies focusing on glacial and interglacial mean states in the equatorial Pacific have alternately suggested that (1) productivity was greater in glacial periods than in interglacial periods [*Pedersen*, 1983; *Sarnthein et al.*, 1987, 1988; *Lyle*, 1988; *Lyle et al.*, 1988; *Pedersen et al.*, 1991; *Thunell et al.*, 1992; *Perks et al.*, 2002; *Richaud et al.*, 2007; *Murray et al.*, 2012] or that (2) productivity was greater in interglacial periods than in glacial periods. [*Pichat et al.*, 2004; *Bradtmiller et al.*, 2006; *Richaud et al.*, 2007; *Costa et al.*, 2016]. Studies encompassing the rapid climate change between glacial and interglacial states have also suggested that (3) the productivity maximum actually occurred during the deglaciation [*Loubere*, 2000; *Bradtmiller et al.*, 2006; *Martinez et al.*, 2006; *Kienast et al.*, 2007; *Anderson et al.*, 2009; *Pichevin et al.*, 2009; *Dubois et al.*, 2010; *Hayes et al.*, 2011; *Rafter and Charles*, 2012; *Winckler et al.*, 2016]. While much of this work is focused on the eastern equatorial Pacific, the records within even this small region do not achieve consensus.

Inconsistencies between these results may reflect real spatial variability in the evolution of equatorial Pacific productivity, but they may also be artifacts of the multitude of proxies and techniques employed, each of which has its own particular biases and limitations. For example, using constant flux proxies, like ^{230}Th, to calculate mass accumulation rates can sometimes reverse previous conclusions derived from age model-based mass accumulation rates [*Paytan et al.*, 1996; *Murray et al.*, 2012; *Winckler et al.*, 2016] which fail to account for the influence of small but systematic errors in age models and postdepositional sediment distribution. In this study, we first reconstruct glacial to Holocene (0–30,000 years ago, or 0–30 ka) productivity (^{231}Pa/^{230}Th) from seven cores near the Line Islands, an understudied region in the central equatorial Pacific that is more likely to capture the mean signal rather than the seasonal upwelling fluctuations prominent in the eastern equatorial Pacific. We then compare these new records with previously published productivity reconstructions (^{231}Pa/^{230}Th, opal fluxes, excess Ba fluxes, and organic carbon fluxes) from across the equatorial Pacific (Figure 1 and Table 1) covering the last 30 kyr to identify coherent patterns in productivity in order to assess how different zones of the equatorial Pacific respond to changing oceanographic conditions.

2. Materials and Methods

In May 2012, the R/V *Marcus G. Langseth* sailed to the Line Islands, where a suite of carbonate-rich cores (>80 wt %) were collected from just south of the equator (0.22°S) to approximately 7°N along the 159°W (±3°) meridian (Figure 1). The seven cores utilized in this study are detailed in Table 1. Core chronologies are based on linear interpolation between 6 and 9 radiocarbon dates [*Costa et al.*, 2016; *Jacobel et al.*, 2016a] as well as oxygen isotopes [*Lynch-Stieglitz et al.*, 2015; *Jacobel et al.*, 2016b]. These cores have sufficiently high sedimentation rates (1.4–3.7 cm/kyr) that 1 cm sampling over the deglacial interval can temporally resolve multimillennial shifts in productivity. While appropriate for reconstructing trends in productivity during the deglaciation, millennial scale events are likely to be affected by bioturbation, which mutes the apparent intensity [*Anderson*, 2001] and extends the apparent duration [*Trauth*, 2013] of these events. We interpret these records with caution on short time scales.

A total of 302 samples from seven cores were analyzed for thorium (^{230}Th, ^{232}Th), uranium (^{238}U, ^{235}U, ^{234}U), and protactinium (^{231}Pa) by isotope dilution inductively coupled plasma mass spectrometry (ICP-MS). Samples (200 mg) were spiked with ^{229}Th, ^{236}U, and ^{233}Pa and processed with complete acid digestion and column chromatography [*Fleisher and Anderson*, 2003]. Isotopes were measured on an Element 2 ICP-MS at the Lamont-Doherty Earth Observatory of Columbia University. Replicates of the internal standard ($n = 23$) indicate that measurements are reproducible within <5% for all isotopes. Excess initial ^{230}Th (or ^{230}Th$_{xs}^0$) and ^{231}Pa (^{231}Pa$_{xs}^0$) concentrations were calculated by correcting for supported decay from lithogenic and authigenic uranium [*Henderson and Anderson*, 2003].

A constant flux proxy, ^{230}Th, is produced in the water column by ^{234}U decay ($\beta = 0.02556$ disintegrations per minute/m^3 yr) and rapidly scavenged by particles falling to the seafloor. The export of this ^{230}Th occurs without its parent uranium isotope so that the ^{230}Th is unsupported, or "excess," in the sediment. Excess ^{230}Th (^{230}Th$_{xs}$) accumulates at a constant rate dependent on the production from uranium and the water depth ($F_{230Thxs} = \beta \times z$). It is subsequently diluted by the bulk flux (BF) of other particles, so that the concentration of ^{230}Th$_{xs}$ varies as an inverse function of the BF: [^{230}Th$_{xs}$] = $\beta \times z$/BF [*Henderson and Anderson*, 2003]. The advantages of ^{230}Th normalization are (1) quantification of absolute particle fluxes, (2) elimination of dilution effects, (3) insensitivity to small errors in age model (about 1%/kyr), and (4) correction for lateral sediment inputs (e.g., focusing and winnowing). Although ^{230}Th normalization has been a topic of considerable debate in the equatorial Pacific [*Lyle et al.*, 2005, 2007, 2014; *Francois et al.*, 2007; *Marcantonio et al.*, 2014], the applicability of this technique has been justified in extensive detail [*Mollenhauer et al.*, 2006, 2011; *McGee et al.*, 2010; *Costa and McManus*, 2017], including across the equatorial Pacific [*Pichat et al.*, 2004; *Anderson et al.*, 2006, 2008; *Kienast et al.*, 2007; *McGee et al.*, 2007, 2010, *Winckler et al.*, 2008, 2016] and particularly at the Line Islands [*Costa et al.*, 2016; *Jacobel et al.*, 2016a, 2016b].

^{231}Pa, like ^{230}Th, is produced by uranium (^{235}U) decay in the water column and scavenged by particles settling to the seafloor. While ^{230}Th scavenging is highly efficient and nearly all the ^{230}Th produced in the water column is exported to the sediment, the same is not true for ^{231}Pa. Scavenging of ^{231}Pa from the water column is much less effective, and it can be dependent on both the particle flux [*Anderson et al.*, 1983, 1990;
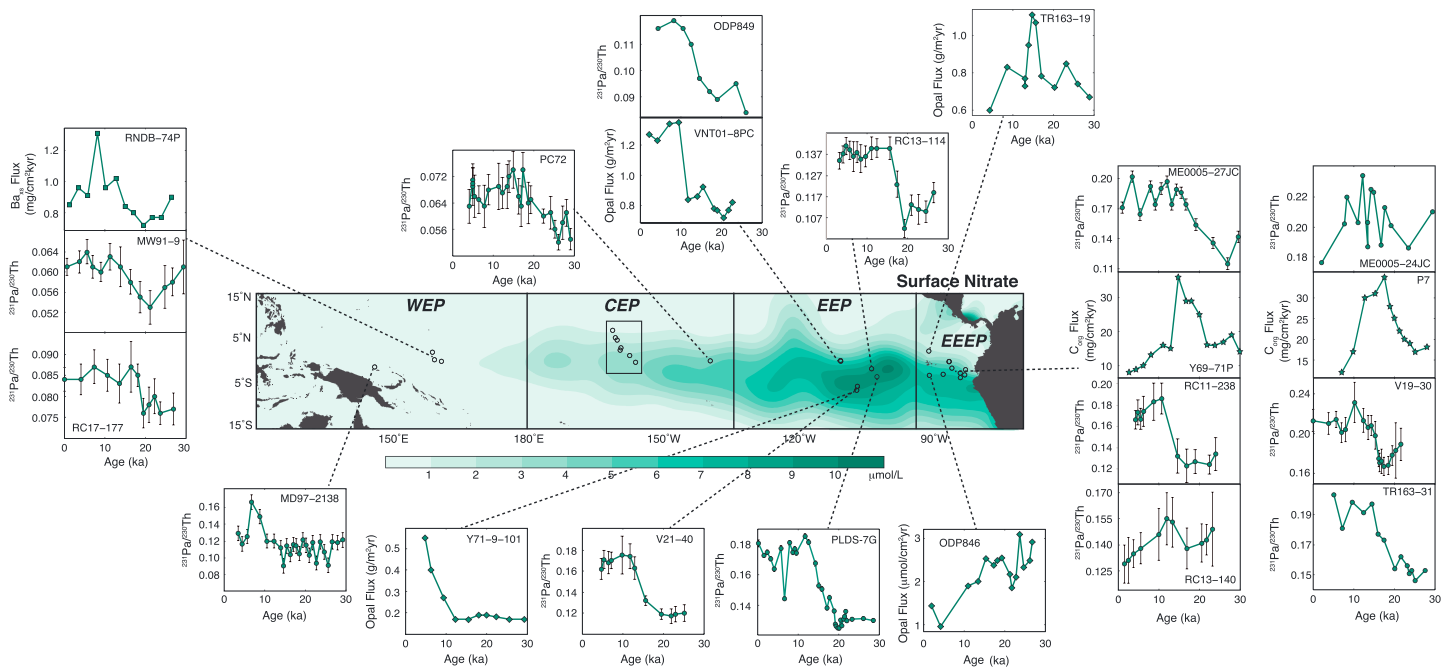
Figure 1. Core locations and previously published productivity records for the equatorial Pacific spanning the past 30 kyr. Black frame indicates the Line Islands (this study). References for the previously published records are included in Table 1. Error bars (2σ) are shown where available; all other errors assumed to be $\leq$10%. Single outlying datapoints have been removed from the following cores: RC13–114, RC13–114, RC11–238, and PLDS-7G to avoid biasing the EOF analysis toward high-frequency anomalies. Most records are ^{231}Pa/^{230}Th (circles), but there are also Ba$_{xs}$ fluxes (squares), opal fluxes (diamonds), and organic carbon fluxes (stars). Dashed lines delineate the easternmost equatorial Pacific (EEEP), eastern equatorial Pacific (EEP), central equatorial Pacific (CEP), and western equatorial Pacific (WEP). Base map is composed of surface nitrate concentrations from World Ocean Atlas 2013.

Bacon, 1988; *Hayes et al.*, 2013] and the particle composition [*Chase et al.*, 2002, 2003; *Geibert and Usbeck*, 2004; *Kretschmer et al.*, 2011]. In regions with low particle flux, ^{231}Pa will escape scavenging, and particles will likely acquire a ^{231}Pa/^{230}Th ratio much lower than that of production in the water column (β_{231Pa}/β_{230Th} = 0.093; activity ratio). In regions of high particle flux, ^{231}Pa will be more efficiently scavenged so that particles acquire high ^{231}Pa/^{230}Th ratios, potentially greater than production. Similarly, opal has a particular affinity for ^{231}Pa, so that opal rich sediments will tend to have high ^{231}Pa concentrations and possibly high ^{231}Pa/^{230}Th ratios greater than production (^{231}Pa/^{230}Th > 0.093). Because high particle fluxes and opal rich sediment characterize high productivity zones, ^{231}Pa/^{230}Th may be used as a proxy for surface productivity. The main advantage of ^{231}Pa/^{230}Th over other productivity proxies, like opal, excess Ba, or organic C fluxes, is its relative insensitivity to changes in preservation and diagenesis [*Chase et al.*, 2003; *Pichat et al.*, 2004]. Comparisons between ^{231}Pa/^{230}Th and other productivity proxies like opal and barite fluxes demonstrate its utility as a proxy for total surface productivity in the Line Islands sediment cores [*Costa et al.*, 2016].

To assess the regional patterns of productivity, an empirical orthogonal function (EOF) analysis was conducted on a total of 28 records from the equatorial Pacific (Table 1). Records were selected based on the following criteria: (1) average temporal resolution was better than 2.5 kyr and (2) the productivity indicator was normalized to a constant flux proxy, ^{230}Th$_{xs}^{0}$. The equatorial Pacific is divided into four subregions: the easternmost equatorial Pacific (EEEP, <95°W, $n = 10$), the eastern equatorial Pacific (EEP, 95–135°W, $n = 6$), the central equatorial Pacific (CEP, 135–180°W, $n = 8$), and the western equatorial Pacific (WEP, 140–180°E, $n = 4$). Because the new Line Islands records have a basis in ^{231}Pa and ^{230}Th systematics, we chose to keep the comparison consistent by focusing exclusively on other records that similarly utilize ^{230}Th systematics when calculating biogenic fluxes. Age models are employed as previously published, and the initial range of resolutions was 460 years to 2500 years, averaging about 1630 years. Single outlying datapoints with high measurement uncertainty have been removed from the following cores: RC13–114, RC13–140, RC11–238, and PLDS-7G (as in Figure 1) in order to not bias the analysis toward high-frequency anomalies. Prior to

Table 1. Core Locations Included in This Study

| Core	Latitude (°N)	Longitude (°E)	Depth (m)	Proxy Data	Sedimentation Rate (cm/kyr)	Reference
MD97–2138	−1.25	146.23	1900	^{231}Pa/^{230}Th	10.8	Pichat et al. [2004]
RC17–177	2.00	159.00	2600	^{231}Pa/^{230}Th	2.0	Bradtmiller et al. [2006]
RNDB-74P	0.34	159.45	2547	Ba$_{xs}$ Flux	2.1	Schwarz et al. [1996]
MW91–9-GGC48	0.00	161.00	3400	^{231}Pa/^{230}Th	2.3	Bradtmiller et al. [2006]
ML1208-36 BB	6.83	198.96	2859	^{231}Pa/^{230}Th	1.8	This Study
ML1208-32 BB	5.20	199.57	2933	^{231}Pa/^{230}Th	2.1	This Study
ML1208-31 BB	4.68	199.95	2857	^{231}Pa/^{230}Th	3.7	This Study
ML1208-25 BB	2.46	200.61	3545	^{231}Pa/^{230}Th	1.8	This Study
ML1208-28 BB	2.97	200.80	3152	^{231}Pa/^{230}Th	3.0	This Study
ML1208-20 BB	1.27	202.74	2850	^{231}Pa/^{230}Th	2.9	This Study
ML1208-13 BB	−0.22	204.04	3049	^{231}Pa/^{230}Th	2.3	This Study
TT013-PC72	0.10	220.60	4298	^{231}Pa/^{230}Th	3.0	Bradtmiller et al. [2006]
ODP849	0.19	249.48	3851	^{231}Pa/^{230}Th	4.4	Pichat et al. [2004]
VNT01-8PC	0.03	249.52	3791	Opal Flux	2.7	Kienast et al. [2006]
Y71–9-101	−6.38	253.07	3175	Opal Flux	3.4	Kienast et al. [2006]
V21–40	−5.52	253.23	3182	^{231}Pa/^{230}Th	4.6	Bradtmiller et al. [2006]
RC13–114	−1.65	256.37	3436	^{231}Pa/^{230}Th	3.6	Bradtmiller et al. [2006]
PLDS-7G	−3.39	257.55	3253	^{231}Pa/^{230}Th	2.6	
TR163–19	2.26	269.05	2348	Opal Flux	4.3	Kienast et al. [2006]
ODP846	-3.10	269.18	3307	Opal Flux	4.6	Richaud et al. [2007]
RC13–140	−2.87	272.25	2246	^{231}Pa/^{230}Th	5.8	Bradtmiller et al. [2006]
Y69-71P	−0.10	273.52	2740	C$_{org}$ Flux	9.2	Kienast et al. [2007]
ME0005-24JC	−0.02	273.54	2941	^{231}Pa/^{230}Th	15.3	Dubois et al. [2010]
RC11–238	−1.51	274.18	2573	^{231}Pa/^{230}Th	6.0	Bradtmiller et al. [2006]
P7	−2.60	276.01	3085	C$_{org}$ Flux	5.2	Kienast et al. [2007]
TR163–31	−3.60	276.05	3209	^{231}Pa/^{230}Th	12.0	Dubois et al. [2010]
V19–30	−3.00	277.00	3091	^{231}Pa/^{230}Th	9.2	Bradtmiller et al. [2006]
ME0005-27JC	−1.85	277.21	2203	^{231}Pa/^{230}Th	6.4	Dubois et al. [2010]

analysis, all records were interpolated to 500 years, to minimize the loss of information from the higher-resolution records, and then individually z scored. The results of the EOF analysis are a series of nonoverlapping (orthogonal) modes that reduce the multivariate data set into the most prominent productivity trends over the past 30 kyr. The loading factors reflect the relative importance of a mode at each core site, i.e., the spatial distribution of that mode. To assess the uncertainty in the EOF results, the data set was resampled 1000 times using a randomly determined set of 15 of the 28 available records (about half the spatial resolution) and reanalyzed for the EOF modes.

3. Results

3.1. New ^{231}Pa/^{230}Th Records From the Line Islands

Overall, ^{231}Pa/^{230}Th ratios exhibit weak temporal trends over the last 30 kyr in the central equatorial Pacific (Figure 2). ^{231}Pa/^{230}Th ranges from 0.073 to 0.094 for 13 BB, 0.065 to 0.086 for 20 BB, 0.056 to 0.066 for 25 BB, 0.060 to 0.071 for 28 BB, 0.035 to 0.055 for 31 BB, 0.046 to 0.56 for 32 BB, and 0.040 to 0.055 for 36 BB. All cores show values equal to or below the production ratio (0.093), with the exception of one datapoint in 13 BB (0.094). Instead of a dominant glacial-interglacial transition, most cores show minor fluctuations about their mean values, which generally decrease with distance from the equator (Figure 3). The highest ratios occur at the equator (13 BB, average ^{231}Pa/^{230}Th = 0.083) and low ratios occur at ~7°N (36 BB, average ^{231}Pa/^{230}Th = 0.047). Core 31 BB (4.68°N) is a notable exception to this trend because its average ^{231}Pa/^{230}Th value (0.044) is anomalously low compared to the adjacent cores 32BB (average ^{231}Pa/^{230}Th = 0.051) and 28 BB (average ^{231}Pa/^{230}Th = 0.066).

In addition to the highest ^{231}Pa/^{230}Th ratios, the equatorial core (13 BB) contains the clearest deglacial trend, with low ^{231}Pa/^{230}Th during the Last Glacial Maximum (LGM) monotonically increasing to high ^{231}Pa/^{230}Th in the late Holocene. This progression amounts to an unambiguous 12.5% increase in ^{231}Pa/^{230}Th from the LGM
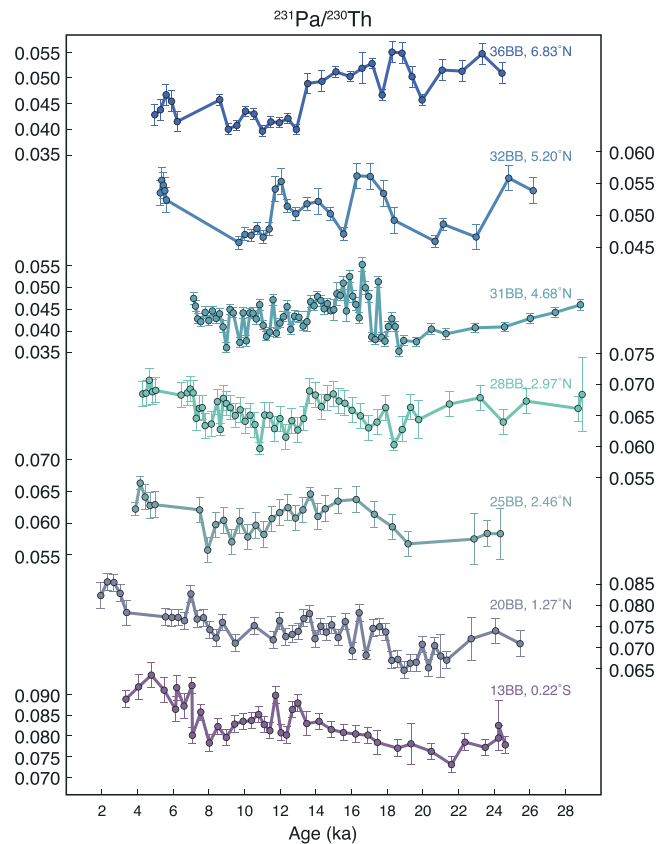
Figure 2. Individual Line Islands $^{231}Pa/^{230}Th$ records, arranged from top to bottom from 7°N (36 BB) southward to the equator (13 BB). Note that each core is displayed on a different y axis scale. Higher $^{231}Pa/^{230}Th$ corresponds to higher productivity. Error bars show 2σ.

to the Holocene. Core 20 BB (1.27°N) displays a similar pattern to 13 BB, as it contains low $^{231}Pa/^{230}Th$ during the LGM increasing directly into high $^{231}Pa/^{230}Th$ in the Holocene, amounting to a 10.2% increase in $^{231}Pa/^{230}Th$. Core 25 BB (2.46°N) has low $^{231}Pa/^{230}Th$ during the LGM and slightly higher $^{231}Pa/^{230}Th$ in the Holocene, but the deglacial pattern is not strictly monotonic. The deglaciation contains a high $^{231}Pa/^{230}Th$ period from ~14 to 16 ka followed by a return to glacial $^{231}Pa/^{230}Th$ values ~8–10 ka before jumping up to the late Holocene high $^{231}Pa/^{230}Th$. The overall change in $^{231}Pa/^{230}Th$ from the LGM to the Holocene is still positive (7.2%), but the progression suggests that high $^{231}Pa/^{230}Th$ may not be unique to interglacial conditions.

Moving northward off the equator, the next three cores (2.97–5.2°N) do not exhibit significant change in $^{231}Pa/^{230}Th$ from the LGM to the Holocene. Core 28 BB (2.97°N) contains a somewhat cyclic pattern in $^{231}Pa/^{230}Th$, with high $^{231}Pa/^{230}Th$ ratios 13.6–15 ka and 4.3–7 ka and low $^{231}Pa/^{230}Th$ ratios 17–18.8 ka

and 10.9–12.3 ka. Core 31 BB (4.68°N) displays a similar pattern to 28BB, with minimal change between the LGM and the Holocene and substantial variability in $^{231}Pa/^{230}Th$ during the deglaciation. In particular, core 31 BB shows a distinct early deglacial peak in $^{231}Pa/^{230}Th$ (16.6–17.5 ka) that rises rapidly out of the LGM and declines gradually into the Holocene. Core 32 BB (5.2°N) contains two deglacial productivity peaks, 16.3–17.0 ka and ~11.7–12.1 ka, the former of which may correspond to the deglacial peak observed in core 31 BB.
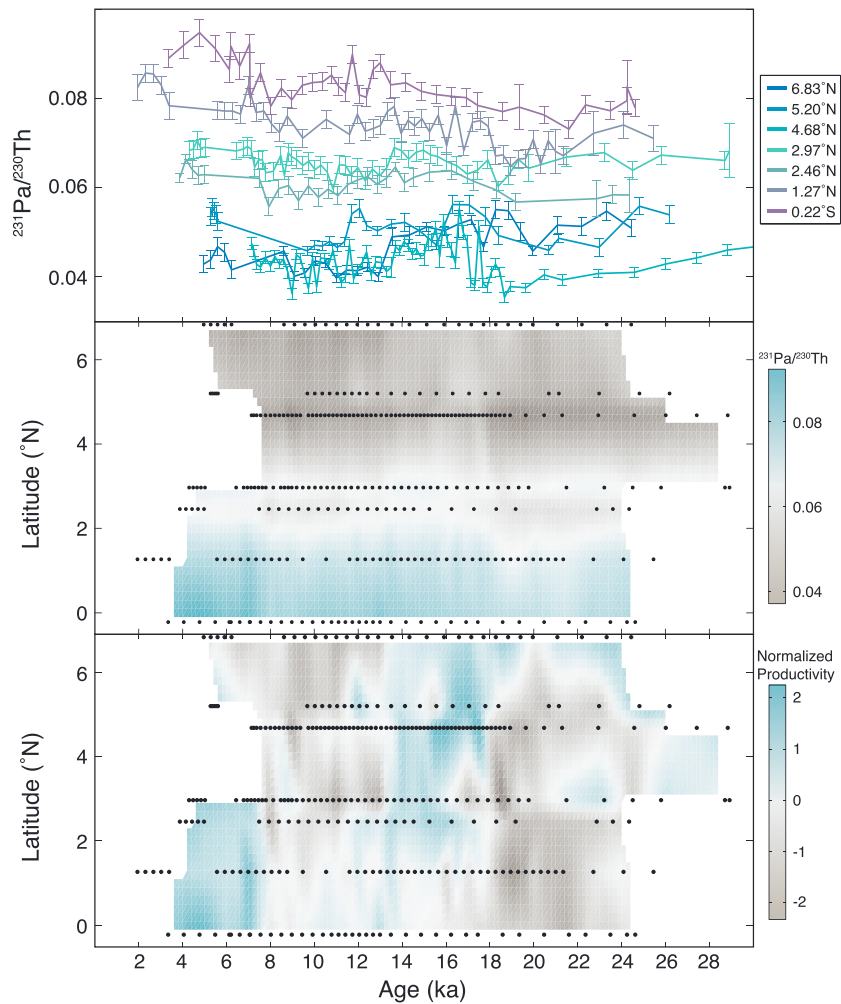
Finally, core 36 BB (6.83°N) has high $^{231}Pa/^{230}Th$ during the LGM and a peak in $^{231}Pa/^{230}Th$ around 18 ka. $^{231}Pa/^{230}Th$ then slowly declines during the deglaciation until a steep dropoff from 12.9–13.5 ka, followed by low values during the Holocene. Unlike the other six cores investigated here, 36 BB is the only core to present a decline (16%) in $^{231}Pa/^{230}Th$ over time, suggesting that productivity decreased from the LGM to the Holocene.

3.2. EOF Analysis of All Cores Across the Equatorial Pacific

The EOF analysis establishes three major modes of deglacial productivity that jointly explain about 74% of the variability in the 28 records from the equatorial Pacific (Figures 4 and 5). The first mode explains about half the variability (48.9 ± 4.8%) with a productivity minimum at the LGM and a maximum in the mid-Holocene ~5 ka. It is particularly evident in the central and western equatorial Pacific, while the opposite pattern of a glacial maximum and mid-Holocene minimum is more prominent in the eastern equatorial Pacific. The second mode (15.5 ± 2.7%) identifies a prominent deglacial productivity peak around 15 ka with very little difference between the LGM and the Holocene productivity values. The spatial pattern is somewhat nondistinct, but the mode seems to be most important at open ocean sites. The third mode (9.8 ± 1.7%) contains productivity peaks every 10 kyr at 0, 10, 20, and 30 ka, and productivity reaches its maximum at ~10 ka. This

Figure 3. (top) Line Islands productivity records compiled onto the same *y* axis scale. Color map is the same as in Figure 2. (middle) Productivity map showing the latitudinal trends in ^{231}Pa/^{230}Th (color bar on right) over time. High productivity (blue) extends to about 1.5–2°N throughout the deglaciation, and a strong N-S productivity gradient is apparent. (bottom) Same as Figure 3 (middle) but each record has been normalized (*z* score) to remove the N-S productivity gradient. This normalized productivity (color bar on right) highlights deviations toward higher (blue) and lower (brown) productivity during the deglaciation.

mode is most prominent within the high-nutrient, low-chlorophyll region of the eastern and central equatorial Pacific (see Figure 1). Uncertainty analyses based on 1000 reiterations of the EOF analysis suggest that even if the amplitude may be less well defined, the timing of productivity peaks in Mode 1 and Mode 2 is quite robust.

4. Discussion

At the Line Islands, the dominant spatiotemporal structure is the equator-northward meridional gradient in productivity. Throughout the last 30 kyr, productivity has always been highest at the equator (Figure 3), and the high productivity zone extended consistently to ~1.5–2°N. This spatial trend is much more robust than the various temporal patterns during the deglaciation. Any temporal changes in productivity co-occurred along the suite of cores in such a fashion that the spatial gradient was not disrupted. The steep decline of productivity at 2°N suggests a nutrient front between nutrient-rich upwelling waters and nutrient-deficient surface waters north of 2°N. The position of this front may be sensitive to several parameters, for example, (1) Fe/NO$_3^-$ ratio of upwelled waters, (2) mixed layer depths, (3) nutrient concentrations in upwelled waters, and (4) physical rate of upwelling. The link between subantarctic mode water (SAMW) and the Equatorial
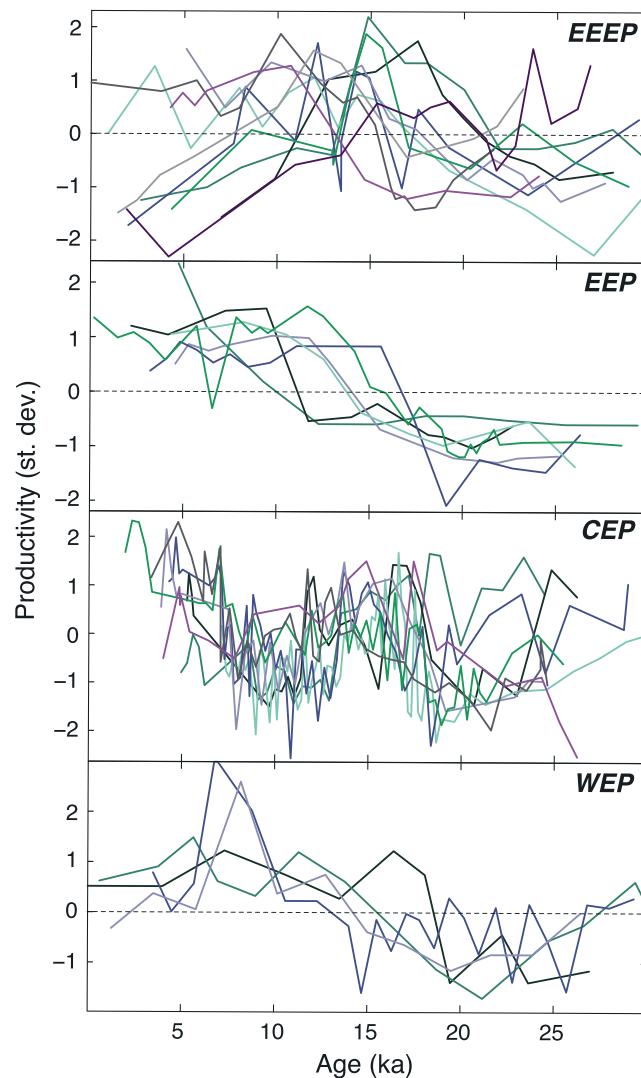
Figure 4. Normalized equatorial Pacific productivity records, organized by subregion (see Figure 1).

Undercurrent (EUC) provides good evidence for increasing nutrient concentrations during the deglaciation (see section 4.1), and so a stable supply of nutrients in upwelling waters on its own cannot explain the static position of the nutrient front. If increasing nutrient concentrations were coupled with, e.g., increasing mixing depth, then the combined effect could lead to a stable net nutrient front as observed at the Line Islands. Alternatively, the static nutrient front may be predominantly reflecting stable rates of upwelling over the past 30 ka. Consistent upwelling rates in the LGM and the Holocene have previously been inferred based on foram-bound $\delta^{15}N$ meridional profiles [*Costa et al.*, 2016], and the similar spatial patterns in productivity through the LGM, deglaciation, and Holocene may permit an extension of this finding throughout the investigated time period. While this interpretation may be speculative, continuing work on meridional sea surface temperature gradients [e.g., *Koutavas and Lynch-Stieglitz*, 2005; *Kienast et al.*, 2013; *Dubois et al.*, 2014] will likely provide more conclusive results.

The two cores within the equatorial upwelling zone are the same cores that exhibit a strong glacial to Holocene monotonic increase in productivity. If we can assume the rate of upwelling was constant, this trend may indicate an increase in nutrient concentrations in the upwelling waters over time (see section 4.1). On the other hand, the cores outside this upwelling zone show different temporal patterns with higher-frequency variability. Normalizing (*z* score) the seven records to remove the meridional gradient reveals a small peak in productivity that appears to transgress southward from 7°N at 18.6 ka to 2.5°N at 14.1 ka (Figure 3). The incoherent timing of this peak is likely an artifact of bioturbation on the variable sedimentation rates of these cores. The most accurate record of this peak is expected at the highest sedimentation rate core (31 BB, 3.7 cm/kyr), where it occurs ~15–17.5 ka. On average $^{231}Pa/^{230}Th$ increased 20 ± 13% in this peak relative to the LGM, a conservative estimate for the change in productivity [*Costa et al.*, 2016], but the high variability of the record within this interval makes it statistically indistinguishable from the LGM-Holocene increase in $^{231}Pa/^{230}Th$ (12 ± 7%) within the same core. The unremarkable amplitude combined with the early deglacial timing contrasts with the deglacial productivity peaks previously observed in the easternmost equatorial Pacific (EEEP), which center ~15 ka and overwhelm the glacial-interglacial variability [e.g., *Kienast et al.*, 2006]. Instead, this early deglacial productivity peak in the central equatorial Pacific may be more related to the secondary 10 kyr cycles in productivity that are sometimes superimposed on glacial-interglacial trends (see section 4.3).
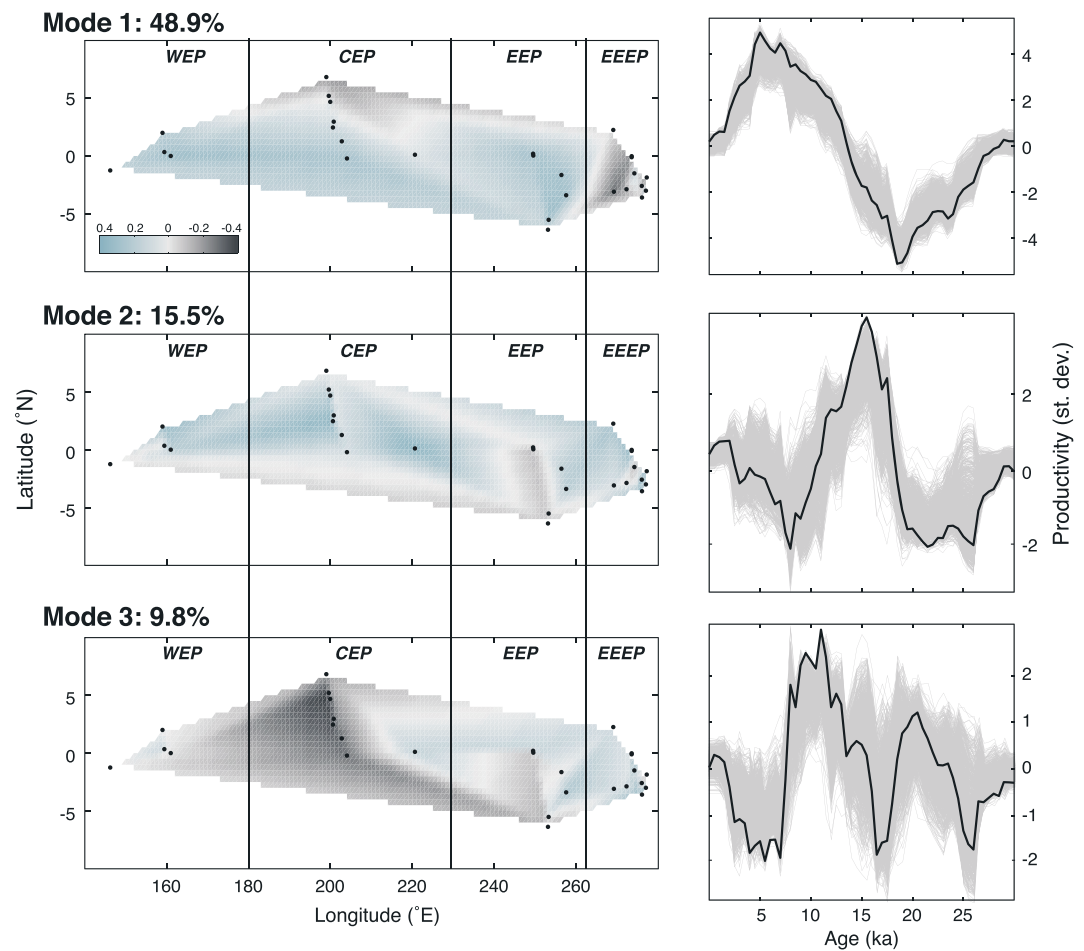
Figure 5. Results of EOF analysis showing (left column) spatial loading factors and (right column) temporal patterns for the first three modes. Loading factors indicate both the sign and intensity of each mode at the different core sites, with blue indicating positive loading and brown indicating negative loading (color bar shown in top panel for all three panels). Full EOF temporal patterns (black line) are shown in the context of the 1000 simulations (gray lines) to demonstrate the robustness of the productivity reconstruction. Because the full EOF analysis included all 28 records while the simulations only included randomly selected 15 of the 28 records, the full EOF temporal patterns are not necessarily equivalent to the mean of the 1000 simulations.

The deglacial productivity patterns observed in the study sites are not unique to the central equatorial Pacific, but they are representative of common patterns recorded across the equatorial Pacific. The EOF analysis distilled the equatorial Pacific records into three modes that together explain over three quarters of the variability in productivity over the last 30 kyr: (1) glacial-interglacial monotonic increase, (2) deglacial peak ~15 ka, and (3) 10 kyr cycles. While this multivariate data reduction technique can identify these dominant trends, it provides no indication for the mechanism(s) driving them. Multiple interpretations of these mechanisms are possible, and below we describe and justify our preferred interpretations. Future work may help pinpoint the most relevant physical processes.

4.1. Mode 1: Nutrient Concentrations

The dominant productivity signal, explaining almost half the variability of the last 30 kyr, is a gradual increase from the glacial period to the Holocene. This pattern was previously noted in the two cores within the equatorial divergence of the Line Islands, where there was no conclusive evidence for substantial changes in the rate of upwelling based on the nearly identical meridional profiles of foraminifera-bound δ^{15}N in the Holocene and last glacial period [*Costa et al.*, 2016]. Here the increase in productivity associated with Mode 1 extends across the equatorial Pacific from 100°W to 150°E and from 5°S to 3°N.

Assuming that upwelling rates are relatively stable across this region, as observed near the Line Islands, this pattern may instead arise from changes in the chemical properties, such as nutrient concentrations, of the upwelling waters over time.

The equatorial Pacific, particularly the EEEP and EEP, is well characterized as Fe limited today [*Coale et al.*, 1996; *Brzezinski et al.*, 2011; *Saito et al.*, 2014], but the greater glacial dust deposition in this region was insufficient to relieve Fe limitation and promote productivity [*Costa et al.*, 2016; *Winckler et al.*, 2016]. With aeolian fluxes of iron eliminated as a primary driver of productivity, changes in upwelling nutrient concentrations are likely to be the dominant control on surface productivity in this region [*Barber and Chavez*, 1991; *Berelson et al.*, 1998; *Chavez et al.*, 1999; *Altabet*, 2001; *Robinson et al.*, 2005; *Strutton et al.*, 2008, 2011].

Upwelling water along the equatorial Pacific comes from the EUC, which travels eastward at 100–150 m water depth, shoaling systematically from west to east. It consists of a deep low-volume, nutrient-rich layer and a shallow high-volume, less nutrient rich layer, which is the major reservoir for upwelling [*Loubere*, 2001]. The EUC is zonally well mixed so that there is no transformation of nutrient concentrations or their isotopic compositions (e.g., δ^{15}N) from west to east across the basin [*Rafter et al.*, 2012]. This homogeneity implies rapid advection of waters through the EUC and, consequently, little chemical difference between waters upwelled at 160°E or 120°W [*Rafter and Charles*, 2012]. Any change in nutrient concentrations within the EUC over time should be recorded simultaneously as a relative increase in nutrients across the equatorial Pacific [*Rafter and Charles*, 2012]. This expectation is consistent with the spatial pattern of Mode 1, in which positive loading factors characterize nearly the entire equatorial region, except at the easternmost part.

The nutrient composition of the EUC is dependent on that of the southern-sourced intermediate waters, which flow northward, shoal through diapycnal mixing within the South Pacific gyre, and ultimately furnish the EUC with nutrients [*Sarmiento et al.*, 2004; *Liu and Alexander*, 2007; *Pena et al.*, 2008; *Rafter et al.*, 2012, 2013; *Rafter and Sigman*, 2016]. The nutrient concentrations of SAMW are determined by the remnants of surface productivity in the subantarctic zone and by entrainment of subsurface waters during the formation of SAMW [*Holte et al.*, 2012, 2013; *Ayers and Strutton*, 2013] and during diapycnal mixing in the South Pacific Gyre [*Rafter et al.*, 2012, 2013; *Rafter and Sigman*, 2016]. Today, nutrient utilization in this region is iron limited, and surplus nutrients are subducted into SAMW, integrated with additional nutrients entrained from deep waters, and transferred to the EUC [*Sarmiento et al.*, 2004; *Martinez and Robinson*, 2010]. During the glacial period, however, abundant atmospheric dust deposition relieved iron limitations in surface waters of the subantarctic zone of the Southern Ocean so that nutrient utilization increased significantly [*Martinez-Garcia et al.*, 2014]. This productivity boon in the Southern Ocean consumed the surplus surface nutrients so that only low residual nutrients were conducted to the equatorial Pacific via SAMW. Furthermore, a weakening or an equatorward shift of the westerlies may have further lowered nutrient concentrations by reducing the entrainment of nitrate and silicate from deep waters [*Kohfeld et al.*, 2013]. Thus, while glacial productivity was high in the subantarctic Southern Ocean, it was low in the WEP, CEP, and EEP [*Costa et al.*, 2016; *Winckler et al.*, 2016].

As nutrient utilization in the subantarctic zone of the Southern Ocean gradually declined during deglaciation and the westerlies weakened and/or moved poleward, nutrient concentrations in the equatorial Pacific rose correspondingly, allowing for the gradual increase in productivity indicated by Mode 1. Increasing nutrient concentrations during the deglaciation have been previously inferred on the basis of foraminiferal δ^{13}C [*Loubere*, 2000; *Spero and Lea*, 2002; *Pena et al.*, 2008], bulk sedimentary δ^{15}N [*Robinson et al.*, 2009; *Galbraith and Jaccard*, 2015], and lower surface pH [*Martinez-Boti et al.*, 2015]. Interestingly, this trend suggests that productivity increased even as aeolian-derived iron fluxes were simultaneously decreasing during the deglaciation [e.g., *McGee et al.*, 2007]. This seeming paradox can be explained by the relatively constant Fe:NO$_3^-$ ratio in upwelling waters that is maintained by the remineralization of sinking organic matter [*Ho et al.*, 2003] as well as sedimentary iron sources from the western Pacific [*Slemons et al.*, 2010, 2012; *Labatut et al.*, 2014; *Qin et al.*, 2016]. As the nutrient concentrations of upwelling waters increased, the iron concentrations of those waters would correspondingly increase as sea level rose and the inundation of shallow sedimentary areas supplied more iron to the EUC. The iron concentrations of upwelling waters far exceed the iron contributions from dust in the equatorial Pacific [*Winckler et al.*, 2016], so that the net change in iron concentrations would be largely determined by that of upwelling waters. Tandem variability of Fe and
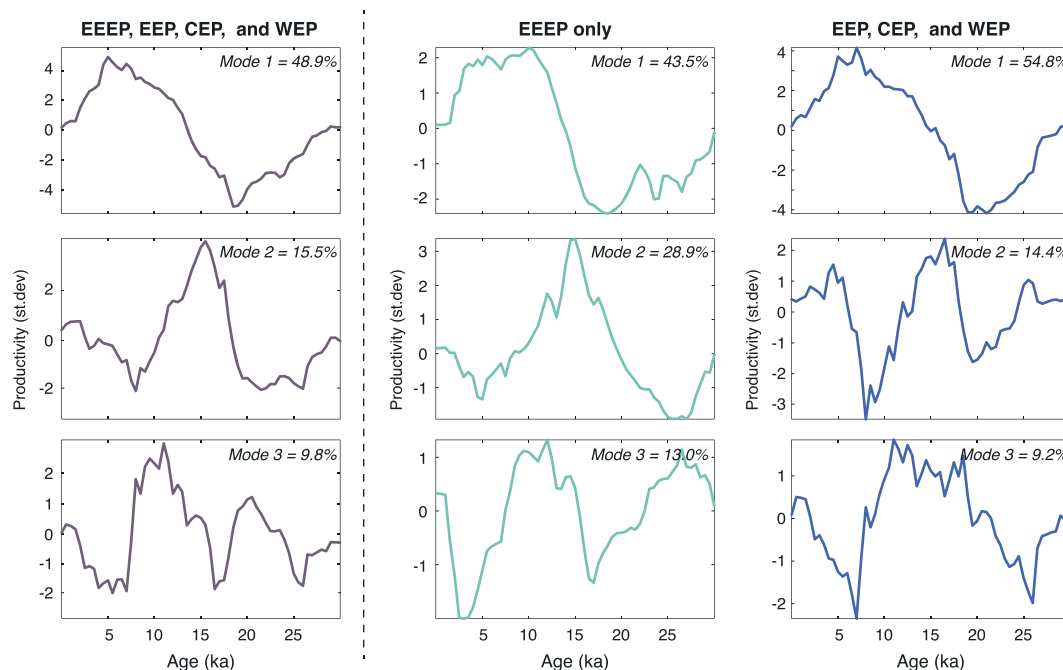
Figure 6. Comparison of EOF analyses in the entire (left column) equatorial Pacific, the (middle column) EEEP only, and the (right column) EEP, CEP, and WEP only. Despite the more variable records within the EEEP, the dominant Mode 1 is quite similar to that observed across the basin as a whole. The unique biogeography of the EEEP instead emerges as greater variance contributed to Modes 2 and 3.

NO_3^- in upwelling waters would allow for an increase in productivity during the deglaciation but would not negate the modern observations of iron limitation, which can only be relieved by an outside source of iron independent of nutrients (e.g., dust or hydrothermal inputs).

The negative factor loading of Mode 1 in the EEEP suggests that locally higher productivity may have occurred near the continental margin during the glacial period. This region is influenced by both equatorial divergence and eastern boundary current upwelling, and so it may not be expected to show the same productivity pattern as the rest of the equatorial Pacific [*Loubere*, 2000]. Indeed, EOF analysis of only the EEEP productivity records demonstrates that Mode 1 is somewhat less important than in the rest of the basin and that Modes 2 and 3 combined explain just as much of the variance as Mode 1 in this region (Figure 6). In addition to the nutrients transported eastward in and upwelled from the EUC, the EEEP nutrient pool may be supplemented by (1) nutrients traveling northward in the Peru current and (2) aeolian and fluvial inputs from the continental margin. Trade winds drive surface waters northward along the coast of Chile and Peru [*Fiedler and Talley*, 2006], and unutilized nutrients within the Peru upwelling system are contributed to the EEEP, so that nutrient utilization increases northward toward the equator [*Doering et al.*, 2016]. Reduced nutrient utilization coupled with reduced or constant productivity in the Peru upwelling system during the last glacial period might increase the export of nutrients from the coast to the equator and contribute an "extra" source of nutrients to the EEEP. Low nutrient utilization and productivity would be consistent with δ^{30}Si and opal flux records along the Peruvian coast [*Ehlert et al.*, 2013; *Doering et al.*, 2016], but large fluctuations in the records and short length of the records (maximum age, 20 ka) may not have been able to capture the true glacial mean state. Alternatively, continentally derived nutrients may have been more important for surface productivity in the EEEP when lower glacial sea level would have permitted transport farther west into the upwelling region. An evaluation of the source behind these extra nutrients in the EEEP is beyond the scope of this paper, but the distinct biogeochemistry of this region presents an oceanographic mystery that comprises a specific directive for future research. At this time, the localized productivity pattern of the EEEP in Mode 1 seems to indicate that divergent reconstructions of productivity in the eastern equatorial Pacific may be a consequence of localized responses to distinct nutrient regimes.

4.2. Mode 2: Equatorial Divergence and Upwelling Rates

The second mode, a productivity peak at 15 ka, explains about 15% of the variability in productivity across the equatorial Pacific during the deglaciation, less than a third of what can be attributed to Mode 1. This mode is almost entirely driven by the records from the EEEP, in which it explains almost 30% of the variance in productivity (Figure 6). Outside of the EEEP, the ~15 ka peak associated with this mode is only slightly greater than the productivity in the glacial period and the late Holocene, and it is identifiable primarily by the deep productivity troughs that flank it. Rather than a gradual transition between glacial and interglacial states, Mode 2 more likely represents a transient instability in response to the changing climate in that interval. The deglacial period is associated with rapid reorganizations of atmospheric and oceanic circulation [e.g., *McManus et al.*, 2004; *Piotrowski et al.*, 2004; *Anderson et al.*, 2009; *Jacobel et al.*, 2016b] that can temporarily but acutely alter the nutrient concentrations and thus the productivity in upwelling waters.

During the deglaciation, cooling of the Northern Hemisphere during Heinrich Stadial 1 (HS1) shifted the Southern Hemisphere westerlies poleward [*Toggweiler et al.*, 2006; *Denton et al.*, 2010], overturning the previously stratified waters of the Southern Ocean. Enhanced Ekman transport and upwelling intensity deliver nutrient rich circumpolar deep water [*Martinez-Boti et al.*, 2015], releasing CO_2 back into the atmosphere and ventilating the deep oceans [*Anderson et al.*, 2009; *Burke and Robinson*, 2012; *Allen et al.*, 2015; *Galbraith and Jaccard*, 2015]. These nutrient-rich deep waters first generated increased opal production south of the Antarctic Polar Front [*Anderson et al.*, 2009] before entrainment into SAMW traveling northward to the EUC and into AAIW heading toward the tropical Atlantic [*Poggemann et al.*, 2017]. In the equatorial Pacific, the presence of high-nutrient southern-sourced deep waters during the deglaciation has been observed in the EEP as a peak in productivity [*Kienast et al.*, 2013], a depleted foraminiferal $\delta^{13}C$ signature [*Spero and Lea*, 2002; *Pena et al.*, 2008], lower surface pH (greater surface pCO_2) [*Martinez-Boti et al.*, 2015], and an enriched ϵNd composition [*Pena et al.*, 2013]. High accumulation rate cores in the central and western equatorial Pacific have also been able to capture this deglacial productivity peak [*Hayes et al.*, 2011; *Winckler et al.*, 2016].

Thermocline deepening during the deglaciation may also have contributed to an increased flux of nutrients around 15 ka. The dramatic reduction of Atlantic meridional overturning circulation during HS1 [*McManus et al.*, 2004; *Bradtmiller et al.*, 2014; *Oppo et al.*, 2015] greatly reduced the volume of intermediate water formed in the Northern Hemisphere. To compensate, intermediate water formation in the Southern Ocean may have increased [*Hain et al.*, 2014], leading to a greater volume of southern-sourced intermediate water production [*Hain et al.*, 2014; *Allen et al.*, 2015]. If more intermediate water were exported to the low latitudes, the tropical thermocline would deepen. Reconstructions of thermocline depth have generated conflicting results for the Last Glacial Maximum, with evidence for both a deeper thermocline [*Dinezio et al.*, 2011; *Ford et al.*, 2015] and a shallower thermocline [*Regoli et al.*, 2015]. During the deglaciation, records of the thermocline steepness and the intensity of upwelling suggest a peak in upwelling rates and thermocline thickness at ~15 ka in the EEP [*Shaari et al.*, 2013]. Ecological transfer functions based on foraminifera and coccolithophores are consistent with peak upwelling rates 20–15 ka that subsequently decline from 14 to 8 ka [*Martinez et al.*, 2006], and nutrient utilization ($\delta^{15}N$) coupled with productivity records have also identified a deglacial maximum in nutrient supply and nutrient utilization at 15 ka in the EEP [*Robinson et al.*, 2009; *Rafter and Charles*, 2012]. Although much of this previous work has focused on the EEEP, the spatial variability in Mode 2 suggests that the strongest productivity response to the nutrient rich deep water pulse may occur in the central equatorial Pacific. The loading of this mode appears to be highest at sites with $^{231}Pa/^{230}Th$, indicating that perhaps the nutrient pulse incorporated a higher Si/NO_3 ratio from the entrainment of deep waters. Furthermore, selective sensitivity to opal scavenging may explain why this productivity peak is more pronounced in some records rather than others.

4.3. Mode 3: Precessional Influence on Wind-Driven Upwelling and Thermocline Dynamics

Another potential influence on the rate and depth of equatorial upwelling, particularly in the EEEP, is the position of the Intertropical Convergence Zone (ITCZ). Located where the northern and southern trade winds meet, the ITCZ is characterized by intense convection, heavy precipitation, low sea surface pressure, and high sea surface temperature [*Waliser and Gautier*, 1993; *McGee et al.*, 2007; *Nicholson*, 2009; *Schneider et al.*, 2014]. The ITCZ migrates seasonally, favoring each hemisphere in its respective summer [*Broccoli et al.*, 2006; *Kang et al.*, 2008], and today, the mean ITCZ is located ~10°N in the eastern Pacific [*Waliser and Gautier*, 1993]. When the ITCZ shifts southward during boreal winter, the primarily vertical winds within the ITCZ suppress

the strong easterlies that normally drive upwelling in the EEEP [*Dubois et al.*, 2014], simulating El Niño-like conditions [*Clement et al.*, 1999]. This more southerly position of the ITCZ is seasonally associated with weaker upwelling, higher sea surface temperatures, and reduced surface productivity [*Koutavas and Lynch-Stieglitz*, 2005].

The relationship between the ITCZ and upwelling may persist on longer time scales beyond the seasonal cycle. Because the ITCZ deflects into the warmer hemisphere, long-term variations in the interhemispheric temperature gradient can shift the mean position to the north or to the south. This temperature imbalance can be associated with large-scale atmospheric and ocean circulation processes [*Manabe and Stouffer*, 1995; *Vellinga and Wood*, 2002; *Zhang and Delworth*, 2005; *Chiang*, 2009; *Fuckar et al.*, 2013; *Marshall et al.*, 2014], but it can also respond to local insolation [*Koutavas and Lynch-Stieglitz*, 2005; *Schneider et al.*, 2014], which, in the tropics, is dominated by precession. Precessional dynamics in the ITCZ and the affiliated tropical rain belt are well documented in climate records from the tropical continents [e.g., *Gasse*, 2000; *Fleitmann et al.*, 2007; *Berke et al.*, 2012; *Carolin et al.*, 2013].

Pacific reconstructions with precessional and half-precessional cycles [*Beaufort et al.*, 2001; *Koutavas et al.*, 2002; *Martinez et al.*, 2003; *Pena et al.*, 2008; *Ivanova et al.*, 2012; *Rafter and Charles*, 2012] are almost exclusively located in the EEEP and may reflect the consequences of local insolation forcing on the mean state of the El Niño–Southern Oscillation (ENSO) [*Clement et al.*, 1999]. High precession index, when the ITCZ is shifted to the north, corresponds with enhanced upwelling and a more La Niña-like state [*Beaufort et al.*, 2001; *Koutavas et al.*, 2002; *Martinez et al.*, 2003; *Pena et al.*, 2008] leading to greater nutrient delivery and utilization [*Rafter and Charles*, 2012]. Low precession index, when the ITCZ is shifted to the south, damps upwelling and generates a more El Niño-like state [*Beaufort et al.*, 2001; *Koutavas et al.*, 2002; *Martinez et al.*, 2003; *Pena et al.*, 2008] leading to reduced nutrient delivery and utilization [*Rafter and Charles*, 2012]. Additionally, the strong presentation of precessional forcing in the EEEP may be related to its particular sensitivity to seasonal variability compared to the CEP and WEP [*Wang and Fiedler*, 2006; *Rafter and Sigman*, 2016], which would directly link surface productivity to insolation cycles without the intervening ENSO system. The link between ITCZ movement, ENSO dynamics, seasonal variability, and upper ocean biogeochemistry all converge on a productivity response to precessional forcing that would be effected most acutely in the EEEP.

Indeed, the productivity pattern of Mode 3 evokes precessional and half-precessional cycles, with the strongest loading in the EEEP. Of the three modes, Mode 3 has the greatest uncertainty (Figure 5), but it can be interpreted as either three half-precessional peaks at 0, 10, and 20 ka or one precessional peak at 10 ka, with a gradual increase in productivity from 25 ka to 10 ka followed by an abrupt decline at ~8 ka. The more robust productivity maximum at 10 ka coincides with the Northern Hemisphere Holocene Thermal Maximum, which fueled the Green Sahara of the African Humid Period with a mean ITCZ shifted substantially to the north both on land [*de Menocal et al.*, 2000] and in the ocean [*Reimi and Marcantonio*, 2016]. A similar deflection of the ITCZ in the EEEP would have promoted La Niña-like conditions, vitalizing surface productivity, especially in the relatively nutrient-replete conditions inferred from Mode 1 at this time. However, while the spatial loading of Mode 3 is weighted toward the EEEP, even there it accounts for only a minor fraction (13%) of the variability in productivity. Considering the uncertainties on Mode 1 (48.9 ± 4.8%) and Mode 2 (15.5 ± 2.7%), it is possible that Mode 3 is an artifact of the data analysis with no mechanistic significance. At most it would only have a tertiary influence on the trends in productivity. Future work may substantiate the hypothesis that the migration of the ITCZ and its effects on ENSO dynamics can influence productivity in the EEP on precessional time scales.

5. Conclusions

Productivity in the equatorial Pacific has been systematically variable, both spatially and temporally, over the last 30 kyr. The dominant temporal pattern is an increase in productivity from the last glacial period to the Holocene, with some cores presenting a secondary productivity peak at 15 ka. In the eastern equatorial Pacific, there is weak evidence for precessional cycles in productivity that may be associated with the ITCZ and its interactions with ENSO dynamical systems. Overall, productivity changes in the equatorial Pacific can largely be attributed to changes in upwelling nutrient concentrations, which are predominantly controlled by processes occurring in the high latitudes. Together, the three modes indicate that peak

productivity occurred during the deglaciation in the east, where upwelling rates are most influential, and elsewhere across the equatorial Pacific during the Holocene, when upwelling nutrient concentrations were the highest.

References

Allen, K. A., E. L. Sikes, B. Hönisch, A. C. Elmore, T. P. Guilderson, Y. Rosenthal, and R. F. Anderson (2015), Southwest Pacific deep water carbonate chemistry linked to high southern latitude climate and atmospheric CO_2 during the last glacial termination, *Quat. Sci. Rev.*, *122*, 180–191, doi:10.1016/j.quascirev.2015.05.007.

Altabet, M. A. (2001), Nitrogen isotopic evidence for micronutrient control of fractional NO_3^- utilization in the equatorial Pacific, *Limnol. Oceanogr.*, *46*(2), 368–380.

Anderson, D. M. (2001), Attenuation of millennial-scale events by bioturbation in marine sediments, *Paleoceanography*, *16*(4), 352–357, doi:10.1029/2000PA000530.

Anderson, R. F., M. P. Bacon, and P. G. Brewer (1983), Removal of ^{230}Th and ^{231}Pa at ocean margins, *Earth Planet. Sci. Lett.*, *66*, 73–90.

Anderson, R. F., Y. Lao, W. S. Broecker, S. E. Trumbore, H. J. Hofmann, and W. Wolfli (1990), Boundary scavenging in the Pacific Ocean: A comparison of ^{10}Be and ^{231}Pa, *Earth Planet. Sci. Lett.*, *96*, 287–304.

Anderson, R. F., M. Q. Fleisher, and Y. Lao (2006), Glacial-interglacial variability in the delivery of dust to the central equatorial Pacific Ocean, *Earth Planet. Sci. Lett.*, *242*(3–4), 406–414, doi:10.1016/j.epsl.2005.11.061.

Anderson, R. F., M. Q. Fleisher, Y. Lao, and G. Winckler (2008), Modern $CaCO_3$ preservation in equatorial Pacific sediments in the context of late-Pleistocene glacial cycles, *Mar. Chem.*, *111*(1–2), 30–46, doi:10.1016/j.marchem.2007.11.011.

Anderson, R. F., S. Ali, L. Bradtmiller, S. H. H. Nielson, M. Q. Fleisher, B. E. Anderson, and L. H. Burckle (2009), Wind-driven upwelling in the Southern Ocean and the deglacial rise in atmospheric CO_2, *Science*, *323*, 1443–1448.

Ayers, J. M., and P. G. Strutton (2013), Nutrient variability in subantarctic mode waters forced by the Southern Annular Mode and ENSO, *Geophys. Res. Lett.*, *40*, 3419–3423, doi:10.1002/grl.50638.

Bacon, M. P. (1988), Tracers of chemical scavenging in the ocean: Boundary effects and large-scale chemical fractionation, *Philos. Trans. R. Soc. London, Ser. A*, *325*, 147–160.

Baines, S. B., B. S. Twining, S. Vogt, W. M. Balch, N. S. Fisher, and D. M. Nelson (2011), Elemental composition of equatorial Pacific diatoms exposed to additions of silicic acid and iron, *Deep Sea Res., Part II*, *58*(3–4), 512–523, doi:10.1016/j.dsr2.2010.08.003.

Barber, R. T., and F. P. Chavez (1991), Regulation of primary productivity rate in the equatorial Pacific, *Limnol. Oceanogr.*, *36*(8), 1803–1815, doi:10.4319/lo.1991.36.8.1803.

Beaufort, L., T. De Garidel-Thoron, and A. C. Mix (2001), ENSO-like forcing on oceanic primary production during the late Pleistocene, *Science*, *293*, 2440–2445.

Berelson, W. M., et al. (1998), Biogenic budgets of particle rain, benthic remineralization and sediment accumulation in the equatorial Pacific, *Deep Sea Res., Part II*, *44*(9), 2251–2282.

Berke, M. A., T. C. Johnson, J. P. Werne, S. Schouten, and J. S. Sinninghe Damsté (2012), A mid-Holocene thermal maximum at the end of the African Humid period, *Earth Planet. Sci. Lett.*, *351–352*, 95–104.

Bradtmiller, L. I., R. F. Anderson, M. Q. Fleisher, and L. H. Burckle (2006), Diatom productivity in the equatorial Pacific Ocean from the last glacial period to the present: A test of the silicic acid leakage hypothesis, *Paleoceanography*, *21*, PA4201, doi:10.1029/2006PA001282.

Bradtmiller, L. I., J. F. McManus, and L. F. Robinson (2014), ^{231}Pa/^{230}Th evidence for a weakened but persistent Atlantic meridional overturning circulation during Heinrich Stadial 1, *Nat. Commun.*, *5*, 5817, doi:10.1038/ncomms6817.

Broccoli, A. J., K. A. Dahl, and R. J. Stouffer (2006), Response of the ITCZ to Northern Hemisphere cooling, *Geophys. Res. Lett.*, *33*, L01702, doi:10.1029/2005GL024546.

Brzezinski, M. A., et al. (2011), Co-limitation of diatoms by iron and silicic acid in the equatorial Pacific, *Deep Sea Res., Part II*, *58*(3–4), 493–511, doi:10.1016/j.dsr2.2010.08.005.

Burke, A., and L. F. Robinson (2012), The Southern Ocean's role in carbon exchange during the last deglaciation, *Science*, *335*(6068), 557–561, doi:10.1126/science.1208163.

Carolin, S. A., K. M. Cobb, J. F. Adkins, B. Clark, J. L. Conroy, S. Lejau, J. Malang, and A. A. Tuen (2013), Varied response of western Pacific hydrology to climate forcings over the last glacial period, *Science*, *340*(6140), 1564–1566, doi:10.1126/science.1233797.

Chase, Z., R. F. Anderson, M. Q. Fleisher, and P. W. Kubik (2002), The influence of particle composition and particle flux on scavenging of Th, Pa and Be in the ocean, *Earth Planet. Sci. Lett.*, *204*, 215–229.

Chase, Z., R. F. Anderson, M. Q. Fleisher, and P. W. Kubik (2003), Scavenging of ^{230}Th, ^{231}Pa and ^{10}Be in the Southern Ocean (SW Pacific sector): The importance of particle flux and advection, *Deep Sea Res., Part II*, *50*, 739–768.

Chavez, F. P., P. G. Strutton, G. Friederich, R. A. Feely, G. C. Feldman, D. G. Foley, and M. J. McPhaden (1999), Biological and chemical response of the equatorial Pacific Ocean to the 1997–98 El Niño, *Science*, *286*(5447), 2126–2131.

Chiang, J. C. H. (2009), The tropics in paleoclimate, *Annu. Rev. Earth Planet. Sci.*, *37*, 263–297, doi:10.1146/annurev.earth.031208.100217.

Clement, A. C., R. Seager, and M. A. Cane (1999), Orbital controls on the El Niño/Southern Oscillation and the tropical climate, *Paleoceanography*, *14*(4), 441–456.

Coale, K. H., S. E. Fitzwater, R. M. Gordon, K. Johnson, and R. T. Barber (1996), Control of community growth and export production by upwelled iron in the equatorial Pacific Ocean, *Nature*, *379*, 621–624.

Costa, K., and J. McManus (2017), Efficacy of ^{230}Th normalization in sediments from the Juan de Fuca Ridge, northeast Pacific Ocean, *Geochim. Cosmochim. Acta*, *197*, 215–225, doi:10.1016/j.gca.2016.10.034.

Costa, K. M., J. F. McManus, R. F. Anderson, H. Ren, D. M. Sigman, G. Winckler, M. Q. Fleisher, F. Marcantonio, and A. C. Ravelo (2016), No iron fertilization in the equatorial Pacific Ocean during the last ice age, *Nature*, *529*(7587), 519–522, doi:10.1038/nature16453.

Dandonneau, Y., P. Y. Deschamps, J. M. Nicolas, H. Loisel, J. Blanchot, Y. Montel, F. Thieuleux, and G. Bécu (2004), Seasonal and interannual variability of ocean color and composition of phytoplankton communities in the North Atlantic, equatorial Pacific and South Pacific, *Deep. Sea Res., Part II*, *51*(1–3), 303–318, doi:10.1016/j.dsr2.2003.07.018.

de Menocal, P. B., J. Ortiz, T. Guilderson, and M. Sarnthein (2000), Coherent high- and low-latitude climate variability during the Holocene warm period, *Science*, *288*, 2198–2202, doi:10.1126/science.288.5474.2198.

Denton, G. H., R. F. Anderson, J. R. Toggweiler, R. L. Edwards, J. M. Schaefer, and A. E. Putnam (2010), The last glacial termination, *Science*, *328*, 1652–1656.

Dinezio, P. N., A. Clement, G. A. Vecchi, B. Soden, A. J. Broccoli, B. L. O. Bliesner, and P. Braconnot (2011), The response of the Walker circulation to Last Glacial Maximum forcing: Implications for detection in proxies, *Paleoceanography*, 26, 1–21, doi:10.1029/2010PA002083.

Doering, K., Z. Erdem, C. Ehlert, S. Fleury, M. Frank, and R. Schneider (2016), Changes in diatom productivity and upwelling intensity since the Last Glacial Maximum: Response to basin-scale atmospheric and oceanic forcing, *Paleoceanography*, 31, 1453–1473, doi:10.1002/2016PA002936.

Dubois, N., M. Kienast, S. Kienast, S. E. Calvert, R. Franois, and R. F. Anderson (2010), Sedimentary opal records in the eastern equatorial Pacific: It is not all about leakage, *Global Biogeochem. Cycles*, 24, GB4020, doi:10.1029/2010GB003821.

Dubois, N., M. Kienast, S. S. Kienast, and A. Timmermann (2014), Millennial-scale Atlantic/East Pacific sea surface temperature linkages during the last 100,000 years, *Earth Planet. Sci. Lett.*, 396, 134–142, doi:10.1016/j.epsl.2014.04.008.

Ehlert, C., P. Grasse, and M. Frank (2013), Changes in silicate utilisation and upwelling intensity off Peru since the Last Glacial Maximum—Insights from silicon and neodymium isotopes, *Quat. Sci. Rev.*, 72, 18–35, doi:10.1016/j.quascirev.2013.04.013.

Fiedler, P. C., and L. D. Talley (2006), Hydrography of the eastern tropical Pacific: A review, *Prog. Oceanogr.*, 69(2–4), 143–180, doi:10.1016/j.pocean.2006.03.008.

Fleisher, M. Q., and R. F. Anderson (2003), Assessing the collection efficiency of Ross Sea sediment traps using [230]Th and [231]Pa, *Deep Sea Res., Part II*, 50, 693–712.

Fleitmann, D., et al. (2007), Holocene ITCZ and Indian monsoon dynamics recorded in stalagmites from Oman and Yemen (Socotra), *Quat. Sci. Rev.*, 26, 170–188.

Ford, H. L., A. C. Ravelo, and P. J. Polissar (2015), Reduced El Niño–Southern Oscillation during the Last Glacial Maximum, *Science*, 347, 255–258.

Francois, R., et al. (2007), Comment on "Do geochemical estimates of sediment focusing pass the sediment test in the equatorial Pacific?" by M. Lyle et al., *Paleoceanography*, 22, PA1216, doi:10.1029/2005PA001235.

Fuckar, N. S., S. Xie, R. Farneti, E. Maroon, and D. M. W. Frierson (2013), Influence of the extratropical ocean circulation on the Intertropical Convergence Zone in an idealized coupled general circulation model, *J. Clim.*, 26, 4612–4629.

Galbraith, E. D., and S. L. Jaccard (2015), Deglacial weakening of the oceanic soft tissue pump: Global constraints from sedimentary nitrogen isotopes and oxygenation proxies, *Quat. Sci. Rev.*, 109, 38–48, doi:10.1016/j.quascirev.2014.11.012.

Gasse, F. (2000), Hydrological changes in the African tropics since the Last Glacial Maximum, *Quat. Sci. Rev.*, 19(1–5), 189–211, doi:10.1016/S0277-3791(99)00061-X.

Geibert, W., and R. Usbeck (2004), Adsorption of thorium and protactinium onto different particle types: Experimental findings, *Geochim. Cosmochim. Acta*, 68(7), 1489–1501, doi:10.1016/j.gca.2003.10.011.

Hain, M. P., D. M. Sigman, and G. H. Haug (2014), Distinct roles of the Southern Ocean and North Atlantic in the deglacial atmospheric radiocarbon decline, *Earth Planet. Sci. Lett.*, 394, 198–208, doi:10.1016/j.epsl.2014.03.020.

Hayes, C. T., R. F. Anderson, and M. Q. Fleisher (2011), Opal accumulation rates in the equatorial Pacific and mechanisms of deglaciation, *Paleoceanography*, 26, PA1207, doi:10.1029/2010PA002008.

Hayes, C. T., R. F. Anderson, S. L. Jaccard, R. François, M. Q. Fleisher, M. Soon, and R. Gersonde (2013), A new perspective on boundary scavenging in the North Pacific Ocean, *Earth Planet. Sci. Lett.*, 369–370, 86–97, doi:10.1016/j.epsl.2013.03.008.

Henderson, G. M., and R. F. Anderson (2003), The U-series toolbox for Paleoceanography, *Rev. Mineral. Geochem.*, 52, 493–531.

Ho, T.-Y., A. Quigg, Z. V. Finkel, A. J. Milligan, K. Wyman, P. G. Falkowski, and F. M. M. Morel (2003), The elemental composition of some marine phytoplankton, *J. Phycol.*, 39, 1145–1159.

Holte, J. W., L. D. Talley, T. K. Chereskin, and B. M. Sloyan (2012), The role of air-sea fluxes in subantarctic mode water formation, *J. Geophys. Res.*, 117, C03040, doi:10.1029/2011JC007798.

Holte, J. W., L. D. Talley, T. K. Chereskin, and B. M. Sloyan (2013), Subantarctic mode water in the southeast pacific: Effect of exchange across the subantarctic front, *J. Geophys. Res. Oceans*, 118, 2052–2066, doi:10.1002/jgrc.20144.

Ivanova, E. V., L. Beaufort, L. Vidal, and M. Kucera (2012), Precession forcing of productivity in the eastern equatorial Pacific during the last glacial cycle, *Quat. Sci. Rev.*, 40, 64–77, doi:10.1016/j.quascirev.2012.02.020.

Jacobel, A. W., J. F. McManus, R. F. Anderson, and G. Winckler (2016a), Climate-related response of dust flux to the central equatorial Pacific over the past 150 kyr, *Earth Planet. Sci. Lett.*, 457, 160–172.

Jacobel, A. W., J. F. McManus, R. F. Anderson, and G. Winckler (2016b), Large deglacial shifts of the Pacific Intertropical Convergence Zone, *Nat. Commun.*, 7, 1–7, doi:10.1038/ncomms10449.

Kang, S. M., I. M. Held, D. M. W. Frierson, and M. Zhao (2008), The response of the ITCZ to extratropical thermal forcing: Idealized Slab-Ocean experiments with a GCM, *J. Clim.*, 21(14), 3521–3532, doi:10.1175/2007JCLI2146.1.

Kienast, M., S. S. Kienast, S. E. Calvert, T. I. Eglinton, G. Mollenhauer, R. Francois, and A. C. Mix (2006), Eastern Pacific cooling and Atlantic overturning circulation during the last deglaciation, *Nature*, 443, 846–849, doi:10.1038/nature05222.

Kienast, S. S., M. Kienast, A. C. Mix, S. E. Calvert, and R. François (2007), Thorium-230 normalized particle flux and sediment focusing in the Panama Basin region during the last 30,000 years, *Paleoceanography*, 22, PA2213, doi:10.1029/2006PA001357.

Kienast, S. S., T. Friedrich, N. Dubois, P. S. Hill, A. Timmermann, A. C. Mix, and M. Kienast (2013), Near collapse of the meridional SST gradient in the eastern equatorial Pacific during Heinrich Stadial 1, *Paleoceanography*, 28, 663–674, doi:10.1002/2013PA002499.

Kohfeld, K. E., R. M. Graham, A. M. de Boer, L. C. Sime, E. W. Wolff, C. Le Quéré, and L. Bopp (2013), Southern Hemisphere westerly wind changes during the Last Glacial Maximum: Paleo-data synthesis, *Quat. Sci. Rev.*, 68, 76–95, doi:10.1016/j.quascirev.2013.01.017.

Koutavas, A., and J. Lynch-Stieglitz (2005), Variability of the marine ITCZ over the eastern Pacific during the past 30,000 years, in *The Hadley Circulation: Present, Past, and Future*, edited by H. F. Diaz and R. S. Bradley, pp. 347–369, Kluwer Academic, Dordrecht, Netherlands.

Koutavas, A., J. Lynch-Stieglitz, T. M. Marchitto, and J. P. Sachs (2002), El Niño-like pattern in ice age tropical Pacific sea surface temperature, *Science*, 297(5579), 226–230, doi:10.1126/science.1072376.

Kretschmer, S., W. Geibert, M. M. Rutgers van der Loeff, C. Schnabel, S. Xu, and G. Mollenhauer (2011), Fractionation of [230]Th, [231]Pa, and [10]Be induced by particle size and composition within an opal-rich sediment of the Atlantic Southern Ocean, *Geochim. Cosmochim. Acta*, 75(22), 6971–6987, doi:10.1016/j.gca.2011.09.012.

Labatut, M., F. Lacan, C. Pradoux, J. Chmeleff, A. Radic, J. W. Murray, F. Poitrasson, A. M. Johansen, and F. Thil (2014), Iron sources and dissolved-particulate interactions in the seawater of the western equatorial Pacific, iron isotope perspectives, *Global Biogeochem. Cycles*, 28, 1044–1065, doi:10.1002/2014GB004928.

Liu, Z., and M. Alexander (2007), Atmospheric bridge, oceanic tunnel, and global climate teleconnections, *Rev. Geophys.*, 45, RG2005, doi:10.1029/2005RG000172.

Loubere, P. (2000), Marine control of biological production in the eastern equatorial Pacific Ocean, *Nature*, 406, 497–500.

Loubere, P. (2001), Nutrient and oceanographic changes in the eastern equatorial Pacific from the last full glacial to the present, *Glob. Planet. Global Planet. Change*, *29*, 77–98, doi:10.1016/S0921-8181(00)00085-0.

Lyle, M. (1988), Climatically forced organic-carbon burial in equatorial Atlantic and Pacific oceans, *Nature*, *335*, 529–532.

Lyle, M., N. Mitchell, N. Pisias, A. Mix, J. I. Martinez, and A. Paytan (2005), Do geochemical estimates of sediment focusing pass the sediment test in the equatorial Pacific? *Paleoceanography*, *20*, PA1005, doi:10.1029/2004PA001019.

Lyle, M., N. Pisias, A. Paytan, J. I. Martinez, and A. Mix (2007), Reply to comment by R. Francois et al. on "Do geochemical estimates of sediment focusing pass the sediment test in the equatorial Pacific?": Further explorations of [230]Th normalization, *Paleoceanography*, *22*, PA1217, doi:10.1029/2006PA001373.

Lyle, M., F. Marcantonio, W. S. Moore, R. W. Murray, C. Huh, B. P. Finney, D. W. Murray, and A. C. Mix (2014), Sediment size fractionation and focusing in the equatorial Pacific: Effect on [230]Th normalization and paleo flux measurements, *Paleoceanography*, *29*, 747–763, doi:10.1002/2014PA002616.

Lyle, M. W., D. W. Murray, B. P. Finney, J. Dymond, J. M. Robbins, and K. Brooksforce (1988), The record of late Pleistocene biogenic sedimentation in the eastern tropical Pacific Ocean, *Paleoceanography*, *3*(1), 39–59, doi:10.1029/PA003i001p00039.

Lynch-Stieglitz, J., et al. (2015), Glacial-interglacial changes in central tropical Pacific surface seawater property gradients, *Paleoceanography*, *30*, 423–438, doi:10.1002/2014PA002746.

Manabe, S., and R. J. Stouffer (1995), Simulation of abrupt climate change induced by freshwater input to the North Atlantic Ocean, *Nature*, *378*, 165–167.

Marcantonio, F., M. Lyle, and R. Ibrahim (2014), Particle sorting during sediment redistribution processes and the effect on [230]Th-normalized mass accumulation rates, *Geophys. Res. Lett.*, *41*, 5547–5554, doi:10.1002/2014GL060477.

Marshall, J., A. Donohoe, D. Ferreira, and D. McGee (2014), The ocean's role in setting the mean position of the Inter-tropical Convergence Zone, *Clim. Dyn.*, *42*(7–8), 1967–1979, doi:10.1007/s00382-013-1767-z.

Martinez-Boti, M. A., G. Marino, G. L. Foster, P. Ziveri, M. J. Henehan, J. W. B. Rae, P. G. Mortyn, and D. Vance (2015), Boron isotope evidence for oceanic carbon dioxide leakage during the last deglaciation, *Nature*, *518*, 219–222, doi:10.1038/nature14155.

Martinez-Garcia, A., D. M. Sigman, H. Ren, R. F. Anderson, M. Straub, D. A. Hodell, S. L. Jaccard, T. I. Eglinton, and G. H. Haug (2014), Iron fertilization of the Subantarctic Ocean during the last ice age, *Science*, *343*, 1347–1350, doi:10.1126/science.1246848.

Martinez, I., L. Keigwin, T. T. Barrows, and Y. Yokoyama (2003), La Niña-like conditions in the eastern equatorial Pacific and a stronger Choco jet in the northern Andes during the last glaciation, *Paleoceanography*, *18*(2), doi:10.1029/2002PA000877.

Martinez, I., D. Rincon, Y. Yokoyama, and T. Barrows (2006), Foraminifera and coccolithophorid assemblage changes in the Panama Basin during the last deglaciation: Response to sea-surface productivity induced by a transient climate change, *Palaeogeogr. Palaeoclimatol. Palaeoecol.*, *234*(1), 114–126, doi:10.1016/j.palaeo.2005.10.022.

Martinez, P., and R. S. Robinson (2010), Increase in water column denitrification during the last deglaciation: The influence of oxygen demand in the eastern equatorial Pacific, *Biogeosciences*, *7*, 1–9.

McGee, D., F. Marcantonio, and J. Lynch-Stieglitz (2007), Deglacial changes in dust flux in the eastern equatorial Pacific, *Earth Planet. Sci. Lett.*, *257*(1–2), 215–230, doi:10.1016/j.epsl.2007.02.033.

McGee, D., F. Marcantonio, J. F. McManus, and G. Winckler (2010), The response of excess [230]Th and extraterrestrial [3]He to sediment redistribution at the Blake Ridge, western North Atlantic, *Earth Planet. Sci. Lett.*, *299*(1–2), 138–149, doi:10.1016/j.epsl.2010.08.029.

McManus, J. F., R. Francois, J.-M. Gherardi, L. D. Keigwin, and S. Brown-Leger (2004), Collapse and rapid resumption of Atlantic meridional circulation linked to deglacial climate changes, *Nature*, *428*(6985), 834–837, doi:10.1038/nature02494.

Mollenhauer, G., J. F. McManus, A. Benthien, P. J. Müller, and T. I. Eglinton (2006), Rapid lateral particle transport in the argentine basin: Molecular ^{14}C and [230]Thxs evidence, *Deep Sea Res., Part I*, *53*(7), 1224–1243, doi:10.1016/j.dsr.2006.05.005.

Mollenhauer, G., J. F. McManus, T. Wagner, I. N. McCave, and T. I. Eglinton (2011), Radiocarbon and [230]Th data reveal rapid redistribution and temporal changes in sediment focussing at a North Atlantic drift, *Earth Planet. Sci. Lett.*, *301*(1–2), 373–381, doi:10.1016/j.epsl.2010.11.022.

Moore, J. K., S. C. Doney, and K. Lindsay (2004), Upper ocean ecosystem dynamics and iron cycling in a global three-dimensional model, *Global Biogeochem. Cycles*, *18*, GB4028, doi:10.1029/2004GB002220.

Murray, R. W., M. Leinen, and C. W. Knowlton (2012), Links between iron input and opal deposition in the Pleistocene equatorial Pacific Ocean, *Nat. Geosci.*, *5*(4), 270–274, doi:10.1038/ngeo1422.

Nicholson, S. E. (2009), A revised picture of the structure of the "monsoon" and land ITCZ over West Africa, *Clim. Dyn.*, *32*(7–8), 1155–1171, doi:10.1007/s00382-008-0514-3.

Oppo, D. W., W. B. Curry, and J. F. McManus (2015), What do benthic δ^{13}C and δ^{18}O data tell us about Atlantic circulation during Heinrich Stadial 1?, *Paleoceanography*, *30*, 353–368, doi:10.1002/2014PA002667.

Park, J. Y., J. S. Kug, J. Park, S. W. Yeh, and C. J. Jang (2011), Variability of chlorophyll associated with El Niño–Southern Oscillation and its possible biological feedback in the equatorial Pacific, *J. Geophys. Res.*, *116*, C10001, doi:10.1029/2011JC007056.

Paytan, A., M. Kastner, and F. P. Chavez (1996), Glacial to interglacial fluctuations in productivity in the equatorial Pacific as indicated by marine barite, *Science*, *274*(5291), 1355–1357.

Pedersen, T. F. (1983), Increased productivity in the eastern equatorial Pacific during the Last Glacial Maximum (19000–14000 yr B.P.), *Geology*, *11*(1971), 16–19.

Pedersen, T. F., B. Nielsen, and M. Pickering (1991), Timing of late Quaternary productivity pulses in the Panama Basin and implications for atmospheric CO2, *Paleoceanography*, *6*(6), 657–677, doi:10.1029/91PA02532.

Pena, L. D., I. Cacho, P. Ferretti, and M. A. Hall (2008), El Niño–Southern Oscillation-like variability during glacial terminations and interlatitudinal teleconnections, *Paleoceanography*, *23*, PA3101, doi:10.1029/2008PA001620.

Pena, L. D., S. L. Goldstein, S. R. Hemming, K. M. Jones, E. Calvo, C. Pelejero, and I. Cacho (2013), Rapid changes in meridional advection of Southern Ocean intermediate waters to the tropical Pacific during the last 30 kyr, *Earth Planet. Sci. Lett.*, *368*, 20–32, doi:10.1016/j.epsl.2013.02.028.

Perks, H. M., C. D. Charles, and R. F. Keeling (2002), Precessionally forced productivity variations across the equatorial Pacific, *Paleoceanography*, *17*(3), 1–7, doi:10.1029/2000PA000603.

Pichat, S., K. W. W. Sims, R. Francois, J. F. McManus, S. Brown-Leger, and F. Albarede (2004), Lower export production during glacial periods in the equatorial Pacific derived from ([231]Pa/[230]Th)xs,0 measurements in deep-sea sediments, *Paleoceanography*, *19*, PA4023, doi:10.1029/2003PA000994.

Pichevin, L. E., B. C. Reynolds, R. S. Ganeshram, I. Cacho, L. Pena, K. Keefe, and R. M. Ellam (2009), Enhanced carbon pump inferred from relaxation of nutrient limitation in the glacial ocean, *Nature*, *459*(7250), 1114–1117, doi:10.1038/nature08101.

Piotrowski, A. M., S. L. Goldstein, S. R. Hemming, and R. G. Fairbanks (2004), Intensification and variability of ocean thermohaline circulation through the last deglaciation, *Earth Planet. Sci. Lett.*, *225*(1–2), 205–220, doi:10.1016/j.epsl.2004.06.002.

Poggemann, D., E. C. Hathorne, D. Nürnberg, M. Frank, I. Bruhn, S. Reißig, and A. Bahr (2017), Rapid deglacial injection of nutrients into the tropical Atlantic via Antarctic intermediate water, *Earth Planet. Sci. Lett.*, *463*, 118–126, doi:10.1016/j.epsl.2017.01.030.

Qin, X., L. Menviel, A. Sen Gupta, and E. Sebille (2016), Iron sources and pathways into the Pacific Equatorial Undercurrent, *Geophys. Res. Lett.*, *43*, 9843–9851, doi:10.1002/2016GL070501.

Rafter, P. A., P. J. DiFiore, and D. M. Sigman (2013), Coupled nitrate nitrogen and oxygen isotopes and organic matter remineralization in the Southern and Pacific Oceans, *J. Geophys. Res. Oceans*, *118*, 4781–4794, doi:10.1002/jgrc.20316.

Rafter, P. A., and C. D. Charles (2012), Pleistocene equatorial Pacific dynamics inferred from the zonal asymmetry in sedimentary nitrogen isotopes, *Paleoceanography*, *27*, PA3102, doi:10.1029/2012PA002367.

Rafter, P. A., and D. M. Sigman (2016), Spatial distribution and temporal variation of nitrate nitrogen and oxygen isotopes in the upper equatorial Pacific Ocean, *Limnol. Oceanogr.*, *61*(1), 14–31, doi:10.1002/lno.10152.

Rafter, P. A., D. M. Sigman, C. D. Charles, J. Kaiser, and G. H. Haug (2012), Subsurface tropical Pacific nitrogen isotopic composition of nitrate: Biogeochemical signals and their transport, *Global Biogeochem. Cycles*, *26*, GB1003, doi:10.1029/2010GB003979.

Regoli, F., T. de Garidel-Thoron, K. Tachikawa, Z. Jian, L. Ye, A. W. Droxler, G. Lenoir, M. Crucifix, N. Barbarin, and L. Beaufort (2015), Progressive shoaling of the equatorial Pacific thermocline over the last eight glacial periods, *Paleoceanography*, *30*, 439–455, doi:10.1002/2014PA002696.

Reimi, M. A., and F. Marcantonio (2016), Constraints on the magnitude of the deglacial migration of the ITCZ in the central equatorial Pacific Ocean, *Earth Planet. Sci. Lett.*, *453*, 1–8, doi:10.1016/j.epsl.2016.07.058.

Richaud, M., P. Loubere, S. Pichat, and R. Francois (2007), Changes in opal flux and the rain ratio during the last 50,000 years in the equatorial Pacific, *Deep. Sea Res., Part II*, *54*(5–7), 762–771, doi:10.1016/j.dsr2.2007.01.012.

Robinson, R. S., D. M. Sigman, P. J. DiFiore, M. M. Rohde, T. A. Mashiotta, and D. W. Lea (2005), Diatom-bound $^{15}N/^{14}N$: New support for enhanced nutrient consumption in the ice age subantarctic, *Paleoceanography*, *20*, PA3003, doi:10.1029/2004PA001114.

Robinson, R. S., P. Martinez, L. D. Pena, and I. Cacho (2009), Nitrogen isotopic evidence for deglacial changes in nutrient supply in the eastern equatorial Pacific, *Paleoceanography*, *24*, PA4213, doi:10.1029/2008PA001702.

Saito, M. A., M. R. McIlvin, D. M. Moran, T. J. Goepfert, G. R. DiTullio, A. F. Post, and C. H. Lamborg (2014), Multiple nutrient stresses at intersecting Pacific Ocean biomes detected by protein biomarkers, *Science*, *345*(6201), 1173–1177, doi:10.1126/science.1256450.

Sarmiento, J. L., N. Gruber, M. A. Brzezinski, and J. P. Dunne (2004), High-latitude controls of thermocline nutrients and low latitude biological productivity, *Nature*, *427*(6969), 56–60, doi:10.1038/nature02127.

Sarnthein, M., K. Winn, and R. Zahn (1987), Paleoproductivity of oceanic upwelling and the effect on atmospheric CO_2 and climatic change during deglaciation times, in *Abrupt Climate Change: Evidence and Implications*, edited by D. W. H. Berger and L. D. Labeyrie, pp. 311–337, D. Reidel, Dordrecht, Netherlands.

Sarnthein, M., K. Winn, J. C. Duplessy, and M. R. Fontugne (1988), Global variations of surface ocean productivity in low and mid latitudes: Influence on CO_2 reservoirs of the deep ocean and atmosphere during the last 21,000 years, *Paleoceanography*, *3*(3), 361–399, doi:10.1029/PA003i003p00361.

Schneider, T., T. Bischoff, and G. H. Haug (2014), Migrations and dynamics of the Intertropical Convergence Zone, *Nature*, *513*(7516), 45–53.

Schwarz, B., and A. Mangini (1996), Geochemistry of a piston core from Ontong Java Plateau (western equatorial Pacific): Evidence for sediment redistribution and changes in paleoproductivity, *Geol. Rundschau*, *85*, 536–545, doi:10.1007/BF02369008.

Shaari, H. B., M. Yamamoto, and T. Irino (2013), Enhanced upwelling in the eastern equatorial Pacific at the last five glacial terminations, *Palaeogeogr. Palaeoclimatol. Palaeoecol.*, *386*, 8–15, doi:10.1016/j.palaeo.2013.03.022.

Slemons, L., B. Paul, J. Resing, and J. W. Murray (2012), Particulate iron, aluminum, and manganese in the Pacific Equatorial Undercurrent and low latitude western boundary current sources, *Mar. Chem.*, *142–144*, 54–67, doi:10.1016/j.marchem.2012.08.003.

Slemons, L. O., J. W. Murray, J. Resing, B. Paul, and P. Dutrieux (2010), Western Pacific coastal sources of iron, manganese, and aluminum to the Equatorial Undercurrent, *Global Biogeochem. Cycles*, *24*, GB3024, doi:10.1029/2009GB003693.

Spero, H. J., and D. W. Lea (2002), The cause of carbon isotope minimum events on glacial terminations, *Science*, *447*, 522–525.

Strutton, P. G., W. Evans, and F. P. Chavez (2008), Equatorial Pacific chemical and biological variability, 1997–2003, *Global Biogeochem. Cycles*, *22*, GB2001, doi:10.1029/2007GB003045.

Strutton, P. G., A. P. Palacz, R. C. Dugdale, F. Chai, A. Marchi, A. E. Parker, V. Hogue, and F. P. Wilkerson (2011), The impact of equatorial Pacific tropical instability waves on hydrography and nutrients: 2004–2005, *Deep Sea Res., Part II*, *58*(3–4), 284–295, doi:10.1016/j.dsr2.2010.08.015.

Thunell, R. C., M. Qingmin, S. E. Calvert, and T. F. Pedersen (1992), Glacial-Holocene biogenic sedimentation patterns in the South China Sea: Productivity variations and surface water pCO_2, *Paleoceanography*, *7*(2), 143–162, doi:10.1029/92PA00278.

Toggweiler, J. R., J. L. Russell, and S. R. Carson (2006), Midlatitude westerlies, atmospheric CO_2, and climate change during the ice ages, *Paleoceanography*, *21*, PA2005, doi:10.1029/2005PA001154.

Trauth, M. H. (2013), TURBO2: A MATLAB simulation to study the effects of bioturbation on paleoceanographic time series, *Comput. Geosci.*, *61*, 1–10, doi:10.1016/j.cageo.2013.05.003.

Turk, D., M. J. McPhaden, A. J. Busalacchi, and M. R. Lewis (2001), Remotely sensed biological production in the equatorial Pacific, *Science*, *293*, 471–474.

Vellinga, M., and R. A. Wood (2002), Global climatic impacts of a collapse of the Atlantic thermohaline circulation, *Clim. Change*, 251–267.

Waliser, D. E., and C. Gautier (1993), A satellite-derived climatology of the ITCZ, *J. Clim.*, *6*, 2162–2174.

Wang, C., and P. C. Fiedler (2006), ENSO variability and the eastern tropical Pacific: A review, *Prog. Oceanogr.*, *69*, 239–266.

Wang, X., J. R. Christian, R. Murtugudde, and A. J. Busalacchi (2006), Spatial and temporal variability in new production in the equatorial Pacific during 1980–2003: Physical and biogeochemical controls, *Deep Sea Res., Part II*, *53*(5–7), 677–697, doi:10.1016/j.dsr2.2006.01.023.

Winckler, G., R. F. Anderson, M. Q. Fleisher, D. McGee, and N. Mahowald (2008), Covariant glacial-interglacial dust fluxes in the equatorial Pacific and Antarctica, *Science*, *320*(5872), 93–96, doi:10.1126/science.1150595.

Winckler, G., R. F. Anderson, S. L. Jaccard, and F. Marcantonio (2016), Ocean dynamics, not dust, have controlled equatorial Pacific productivity over the past 500,000 years, *Proc. Natl. Acad. Sci. U.S.A.*, *113*(22), 6119–6124, doi:10.1073/pnas.1600616113.

Zhang, R., and T. L. Delworth (2005), Simulated tropical response to a substantial weakening of the Atlantic thermohaline circulation, *J. Clim.*, *18*, 1853–1860.